Desalination and Water Treatment
www.deswater.com

doi: 10.5004/dwt.2022.28853

272 (2022) 126–137
October

Removal of phosphorus from wastewater by metal salt doping waste-based ceramsite

Yixiao Xing†, Xiao Huang†, Jianghua Yu*, Chao Gong, Chen Zhang

Collaborative Innovation Center of Atmospheric Environment and Equipment Technology, Jiangsu Key Laboratory of Atmospheric Environment Monitoring and Pollution Control, School of Environmental Science and Engineering, Nanjing University of Information Science & Technology, Nanjing 210044, China, Tel. +86 025-58695677/18751906939; Fax: +86 025-58731090; email: yujh@nuist.edu.cn (J. Yu), Tel. 15136871599; email: xingyx1013@163.com (Y. Xing), Tel. 18825222704; email: huangxiao901231@126.com (X. Huang), Tel. 13016963908; email: 2194561697@qq.com (C. Gong), Tel. 17355338919; email: zcleon@foxmail.com (C. Zhang)

Received 26 February 2022; Accepted 17 August 2022

ABSTRACT

Fly ash (FA) and sewage sludge (SS) as adsorbents have recently developed to remove phosphate in wastewater, doping Al and Fe is an efficient method to improve phosphorus adsorption for ceramsite prepared with FA and SS. In this study, the removal performance of phosphorus by three kinds of ceramsite was investigated under the optimum concentration of Al and Fe salt. Besides, adsorption kinetics and adsorption isotherms were investigated to reveal the adsorption mechanisms. It was found that the best particle strength was obtained when the ratio of fly ash, sludge and concrete was 6:3:2. The adsorption capacity of Al and Fe-doped ceramsite was 669.1 and 458.26 mg kg^{-1}, respectively, which was much higher than that of undoped ceramsite (58.233 mg kg^{-1}). Therefore, the method of metal salt doping waste-based ceramsite can be employed to immobilize phosphate in wastewater.

Keywords: Wastewater; Phosphorus adsorption; Waste-based ceramsite; Fly ash; Sewage sludge

1. Introduction

Water eutrophication has become a major global environmental issue and will continue to pose a major threat to global environmental and human health and cause serious economic losses [1]. The discharge of wastewater containing low concentration phosphorus contributed to the process of water eutrophication. Therefore, the advanced treatment to control wastewater containing phosphorus in the natural water bodies becomes the focus of industrial wastewater treatment. Furthermore, the enormous quantity of solid wastes generated from metallurgy, thermal power generation, and mineral extraction contributes to very serious environmental problems every year. Some of these solid wastes (such as fly ash, red mud, slag, and Fe/Al residual) can effectively absorb phosphate because these materials are enriched with oxides of aluminum, iron and calcium [2,3]. To control the increase of phosphorus load in water and improve the utilization rate of solid waste, it is of great importance to develop useful ways to attenuate the amount of phosphorus in the aquatic environment.

The phosphorus removal for wastewater mainly depends on the biological phosphorus accumulation, chemical precipitation, and adsorption method. Adsorption has been paid more attention owing to its advantages of high efficiency, low energy consumption, simple processing equipment, stable performance of adsorbent, and easy regeneration [4]. For the traditional adsorption process,

* Corresponding author.

† Both the authors contributed equally to this work.

1944-3994/1944-3986 © 2022 Desalination Publications. All rights reserved.

bentonite [5], diatomite [6], and zeolite [7] are the most common adsorbents for treating phosphorus wastewater. And now, the use of solid wastes for phosphorus adsorption is a more promising adsorptive process. Many researchers have begun to use solid waste (such as industrial waste residue, water plant sludge, etc.) to prepare phosphorus removal adsorbents. For instance, Wang et al. [8] developed three kinds of solid waste (fly ash, red mud, and ferric-alum water treatment) as adsorbents to remove phosphorus. Compared with two natural adsorbents (zeolite and diatomite), these three solid wastes possessed a higher adsorption capacity for phosphorus because of the higher Fe, Al, and Ca contents. Thus, developing an industrial waste adsorbent that can not only solve the problem of eutrophication but also reduce the cost of phosphorus removal would help realize the resource utilization of industrial wastes.

Water supply sludge is the residue of a water treatment process for a municipal water plant, the Ca^{2+}, Fe^{3+}, and Al^{3+} contained in water supply sludge can combine with PO_4^{3-} during plasma hydrolysis. The precipitation appears on the surface of the sludge to achieve the purpose of phosphorus removal [9]. A recent study found that the preparation of ceramsite from waterworks sewage and coal fly ash as the adsorbent can remove phosphorus in the secondary effluent of sewage treatment plants [10]. In addition, fly ash is a solid waste with a high adsorption capacity, and it contains a lot of metal oxides such as calcium oxide, magnesium oxide, manganese oxide, iron oxide, etc. Phosphates can be removed by complexing or precipitation of calcium/magnesium phosphate. It owns the characteristics of large specific surface area, porosity, and good phosphorus adsorption performance [11]. Li et al. [12] studied that preparing ceramsite with fly ash, lime and clay as raw materials had a better adsorption capacity for phosphorus. Previous studies have revealed that the ceramsite prepared by composite material had a good removal effect on phosphorus. Furthermore, concrete as industrial waste has low phosphorus background value, low price, porous structure, easy to obtain and so on, which has the potential for phosphorus removal. However, there were few reports on preparing ceramsite with fly ash, sewage sludge, and concrete as the primary raw materials and studying its phosphorus adsorption effect. In addition, there were no reports on the adsorption effect of aluminum (Al) and iron (Fe) salt on the above ceramsite. Thus, it is meaningful to find out whether the doping of Al and Fe is an effective method to improve the phosphorus adsorption for ceramsite prepared with fly ash and sewage sludge.

The work developed a composite material based on construction waste (fly ash, sludge, concrete) doped with metal salts, and applied to adsorb phosphorus from industrial wastewater. It provides a promising technology to solve the problem of phosphorus removal from industrial wastewater and realize the resource utilization of construction waste. This work aimed to reveal the adsorption performance of ceramsite prepared from industrial waste (fly ash, sludge, concrete) and doped with Al and Fe salts on phosphorus in an aqueous solution. First, the optimal particle strength of ceramic prepared from fly ash, sludge, and concrete at different ratios was investigated. Then the adsorption capacity of Al and Fe salts to phosphorus in solution at different concentrations was explored. Finally, the adsorption mechanism of phosphorus in solution by metal doped ceramsite was revealed by adsorption kinetics and adsorption isotherm.

2. Materials and methods

2.1. Material

The fly ash was collected from a power plant, the sewage sludge used in the experiment was collected from a sewage treatment plant sedimentation tank, and the concrete was collected from a construction site in Nanjing. The fly ash, sewage sludge, and concrete were dried and then crushed and ground with a pulverizer, sifted, dried at 40°C, collected and set aside. Detailed information about sewage sludge, fly ash, and main concrete components are shown in Table 1.

2.2. Prepared of waste-based ceramsite

The ceramsite was prepared using fly ash, sewage sludge, and concrete as raw materials. Five ratios of fly ash and clay, that is, 3, 4, 5, 6, and 7, were used for taking 10 g of clay. Five ratios of sewage sludge and clay were used, that is, 1.5, 2, 2.5, 3, and 3.5. Five ratios of concrete and clay were employed, that is, 1, 2, 3, 4, and 5. The raw meal nodules were prepared from sewage sludge, fly ash, concrete, and clay in different proportions, which were mixed into a granulator with a rotating speed of 30–40 rpm. Afterward, the raw meal nodules with a particle size of 4–6 mm were

Table 1
Sewage sludge, fly ash and concrete main components (%)

Chemical composition (%)	Sewage sludge	Fly ash	Concrete
SiO_2	28.36	47.68	23.87
Al_2O_3	8.674	37.78	6.35
TiO_2	–	2.49	–
Fe_2O_3	3.99	4.39	2.21
CaO	2.3	–	57.15
MgO	2.3	0.5	3.2
K_2O	1.7	–	2.15
Na_2O	–	3.27	1.32

screened out, which were oven-dried for 2 h at 105°C to remove moisture. After drying, the raw meal nodules were sintered at 1,150°C for 10 min in a muffle furnace. At last, the ceramsite sample was naturally cooled to room temperature, and the particle strength of the ceramsite was measured. The whole process of waste-based ceramsite preparation is shown in Fig. 1.

At room temperature, the ceramsite was put into the concentration of 0.25, 0.5, 0.75 and 1 mol L^{-1} of Al salt (aluminum nitrate), and Fe salt (ferric chloride) solution. The initial temperature of the metal solution was determined through a water bath, they were placed in a constant temperature shaker with a rotating speed of 120 rpm, the ceramsite was removed after a certain doping time, which was dried in an oven at 60°C. Then it was burned for 4 h in a muffle oven at 600°C. Finally, the ceramsite was cooled at room temperature and stored.

2.3. Experiment of optimal doping conditions

For the optimal doping concentration of Al and Fe salt solution, Fe and Al solution concentrations were 0.25, 0.5, 0.75, and 1 mol L^{-1}, respectively. The ratio of ceramsite mass to the metal salt solution was 1:3, doped for 5 h at 20°C. 2 g of Fe and Al-doped ceramsite were added into KH_2PO_4 solution, respectively (the initial phosphorus = 10 mg L^{-1}). The mixed solution was shaken for 20 h at 25°C. Samples were subjected to measurement of phosphate concentration by potassium persulfate oxidation-molybdenum-antimony anti-spectrophotometric method.

2.4. Phosphorus adsorption experiment

For kinetic studies, 5 g of undoped ceramsite, 2 g of Al-doped ceramsite, and 2 g of Fe-doped ceramsite were weighed, (ensuring a dose of 100 g L^{-1} for undoped ceramsite and 40 g L^{-1} for Al and Fe-doped ceramsite), the initial phosphate of KH_2PO_4 solution was 10 mg L^{-1}, the mixed solution was shaken several times at 25°C. Set the reaction time at a certain interval (0–24 h) to reach the phosphorus adsorption equilibrium. For adsorption isotherm tests, the initial phosphate of KH_2PO_4 solution varied between 2–10 mg L^{-1}. The mixed solution was shaken at 25°C to reach the adsorption equilibrium, and equilibrium adsorption capacity (q_e, mg g^{-1}) was calculated using equation (1).

$$q_e = \frac{(C_0 - C_e)V}{m} \tag{1}$$

where C_0 and C_e (mg L^{-1}) are the initial and equilibrium phosphorus concentrations respectively, V (mL) is the solution volume, and m (g) is the quality of ceramsite.

2.5. Analytical method

Scanning electron microscopy (SEM) and energy-dispersive X-ray spectroscopy (EDS) were obtained on the scanning electron microscope-energy dispersive spectrometer (SEM-EDS) SU8010 (Hitachi, Japan). The X-ray diffraction (XRD) measurement was performed on the PHI-5000 Versaprobe-III system of the electron energy spectrometer (ULVAC-PHI, USA). In the Fourier-transform infrared spectroscopy (FTIR) is5 (Conta Instruments Inc.), the Fourier exchange was used to transform the time-domain function in the interferogram into a frequency-domain function graph.

2.6. Data analysis

2.6.1. Adsorption kinetics

Pseudo-first-order and pseudo-second-order models were used to analyze the kinetic data, Eq. (2) represented the first-order and Eq. (3) described the second-order, which is expressed as:

$$\log(q_e - q_t) = \log q_e - \frac{k_1}{2.303}t \tag{2}$$

$$\frac{t}{q_t} = \frac{1}{k_2 q_e^2} + \frac{1}{q_e}t \tag{3}$$

where q_t and q_e (mg g^{-1}) are the adsorption capacities of phosphorus at time t (min) and equilibrium, respectively. k_1 (h^{-1}) and k_2 (g mg^{-1} h^{-1}) are the rate constants of

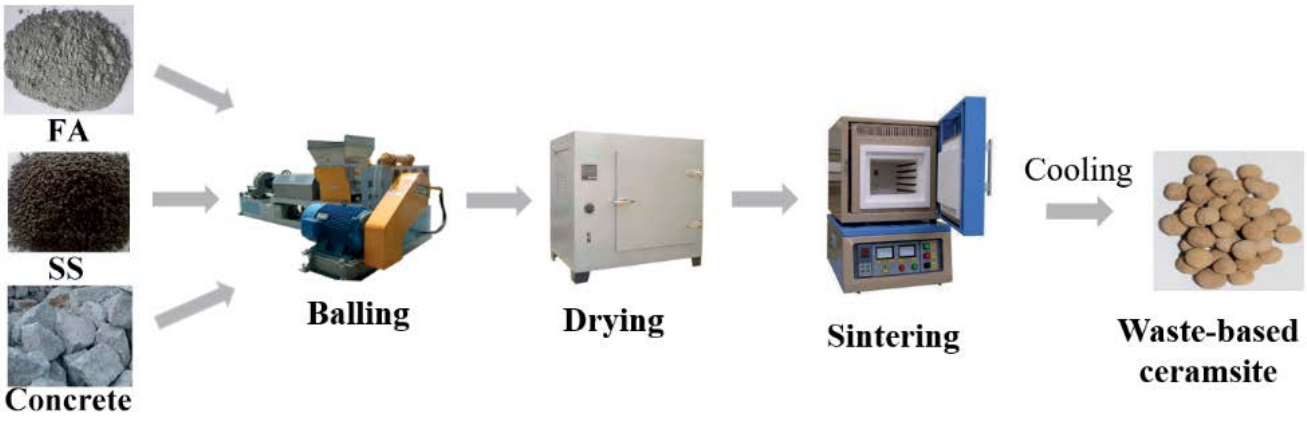

Fig. 1. Whole preparation process of waste-based ceramsite.

the pseudo-first-order and pseudo-second-order kinetic models, respectively.

2.6.2. Adsorption isotherm

The isotherm data were analyzed using Langmuir and Freundlich models, Eq. (4) represents the Langmuir model, and Eq. (5) describes the Freundlich mode, as expressed:

$$q_e = \frac{q_m bc}{1+bc} \tag{4}$$

$$q_e = KC^n \tag{5}$$

where q_e (mg g^{-1}) and C_e (mg L^{-1}) are the phosphorus adsorption capacity and concentration at equilibrium, respectively. And q_m (mg g^{-1}) is the maximum adsorption capacity, K, n, and b are all adsorption constants.

3. Results and discussion

3.1. Strength of waste-based ceramsite

To determine the ratio of each component of the ceramsite, the proportioning test of fly ash, sewage sludge, concrete was carried out.

3.1.1. Ratio of fly ash and clay

It is an effective way for comprehensive utilization of fly ash to prepare fly ash sintered ceramsite, the content of fly ash should be raised as much as possible. Fig. 2a shows the strength of ceramsite particles under different ratios of fly ash and clay. It was obvious that the particle strength enhanced gradually with the proportion of fly ash and clay from 3 to 6, and it declined from 158.76 N to 79.38 N under the ratio reached 7. This might be the fact that aluminum oxide (Al_2O_3) was contained in fly ash, an important component of forming high-strength mullite. So the sample strength was enhanced by the increasing dosing of fly ash [13]. The particle strength of ceramsite largely depended on the content of fly ash, and it decreased when the content of fly ash was higher. Calcium oxide (CaO), ferric oxide (Fe_2O_3), and magnesium oxide (MgO) were impurity phases that affected the sintering of fly ash. As the content of these impurities increased, a large amount of gas produced destroyed the strength of the ceramsite [14]. Therefore, the optimal ratio of fly ash and clay was 6.

3.1.2. Ratio of sewage sludge and clay

The effect of sewage sludge proportion on the strength of ceramsite particles is shown in Fig. 2b. The particle strength gradually increased with the ratio of sewage sludge and clay was from 1.5 up to 3, then dropped from 168.56 N to 118.58 N under the ratio reached 3 and 3.5, respectively. This phenomenon might be due to the presence of a great many silicon dioxides (SiO_2) and Al_2O_3 in sewage sludge. However, the amount of sludge was positive with the content of organic matter, so numerous pores were generated in the high-temperature sintering process, which reduced the particle strength [10,15]. Therefore, the optimal ratio of sewage sludge and clay was 3.

3.1.3. Ratio of concrete and clay

The influence of different concrete and clay ratios on the strength of ceramsite particles is shown in Fig. 2c. It was a growth of particle strength when the ratio of concrete and clay was from 1 to 2. A lot of CaO was contained in concrete, which increased the particle strength as flux. However, it was obvious that the particle strength of ceramsite gradually declined with excessive concrete content. Especially the particle strength of ceramsite was less than 60 N when the ratio reached 5. The decomposition reaction of CaO released carbon dioxide (CO_2), which acted as a micro-expansion agent in the firing process of ceramsite. Cracks in the surface of the ceramsite due to over-expansion, leads to a reduction in the strength of the ceramsite when the ratio of concrete to clay is 3–5. Therefore, the optimal ratio of concrete and clay was 2 under the condition of ensuring a certain particle strength.

In summary, the best ceramsite ratio with fly ash, sewage sludge, and concrete as raw materials were 6:3:2.

3.2. Phosphorus adsorption effect of Al and Fe-doped ceramsite

3.2.1. Concentration of Al and Fe salt solution

Fig. 3a shows the analysis of the phosphorus removal effect. It was observed that the adsorption of phosphorus by doped ceramsite increased with the increase of Al and Fe salt impregnation concentration, which was due to the number of adsorption sites provided by metal cation after doping increased. Since the Fe and Al salt solutions were acidic, the acidity of doped solutions enhanced with the increased Fe and Al salt concentrations. However, the high acidity of the doped solution destroyed the surface and internal skeleton structure of the ceramsite, and reduced the phosphorus removal ability of the material. In addition, it may increase the cost of doping. Therefore, the optimal doping concentration of Al salt and Fe salt were 0.75 mol L^{-1} in this experiment.

3.2.2. Adsorption effect of phosphorus

The phosphorus adsorption capacity of undoped, Al and Fe-doped ceramsite at different reaction times is shown in Fig. 3b. During the whole reaction process, the adsorption capacity of undoped ceramsite increased to 55.09 mg kg^{-1}. In the period of 0–8 h, the adsorption capacity of Al and Fe-doped ceramsite increased to 234.02 and 167.95 mg kg^{-1}, respectively. This phase had the steepest ascent curve, and the adsorption rate was the fastest.

Previous studies showed that the adsorption stage was mainly controlled by the liquid film diffusion process [16]. That is to say, a liquid film was formed on the surface of the doped ceramsite in the solution, which produced a phosphorus concentration difference between the liquid film and the surrounding solution, thereby forming a phosphorus concentration gradient. Besides, the higher

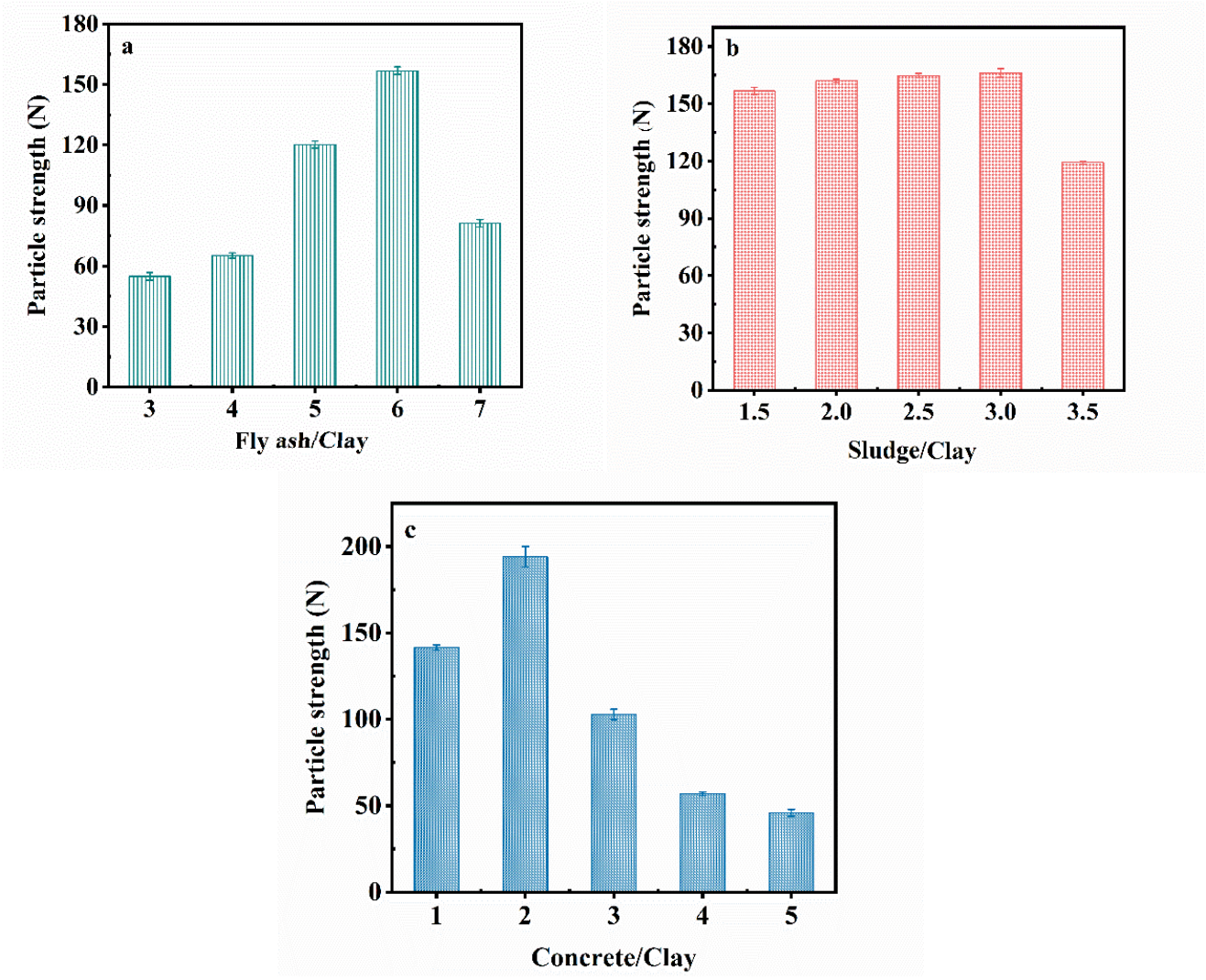

Fig. 2. Influence of the ratio of raw materials on the strength of ceramsite particles: fly ash content (a), sewage sludge content (b) and concrete content (c).

concentration difference led to a greater migration force. The phosphate ions in the solution acted on adsorption sites of ceramsite under the action of this migration force. Moreover, the concentration difference was more considerable in the early stage of adsorption. More specific surface and adsorption sites of ceramsite were exposed in solution to react with phosphate. It might be why the adsorption rate at this stage was the fastest. This was similar to other studies on phosphorus removal using modified diatomite [17], Drinking Water Treatment Sludge (DWTS) [18], and altered zeolite [19].

The second adsorption stage appeared after 8 h. Obviously, the increase in contact time enhanced the adsorption capacity of phosphorus, and the adsorption gradually became slower until equilibration. The adsorption may dominate the phosphorus adsorption inside the pores at this stage [8]. From the change of ceramsite adsorption capacity, it can be found that Al and Fe-doped ceramsite adsorption equilibrium time was 20 h, and the adsorption capacity reached 274.40 and 202.33 mg kg^{-1}, respectively. After 20 h, it was the third stage of adsorption. As the reaction time continued to increase, the undoped ceramsite began to show a desorption trend, while the adsorption capacity of Al and Fe-doped ceramsites almost did not change. Hence, based on the above analysis, the optimum contact time for the adsorption of phosphorus by Al and Fe-doped ceramsite was fixed as 20 h. Compared to the adsorption effects of Al and Fe-doped ceramsites, the phosphorus removal effect was not different within 0–2 h. Nevertheless, the phosphorus removal effect of Al-doped ceramsite was greater than Fe-doped ceramsite in 2–8 h. Two reasons might cause this, on the one hand, aluminum hydroxide [$Al(OH)_3$] colloid formed by aluminum in water can convert negatively charged phosphate PO_4^{3-} into $AlPO_4$ or hydroxy phosphate [$Al(OH)_y(PO_4)_Z$] precipitation to remove phosphorus in the water. However, on the other hand, metallic iron ions' existence depended on the environment's pH value and redox condition. Besides, changing the redox condition of iron

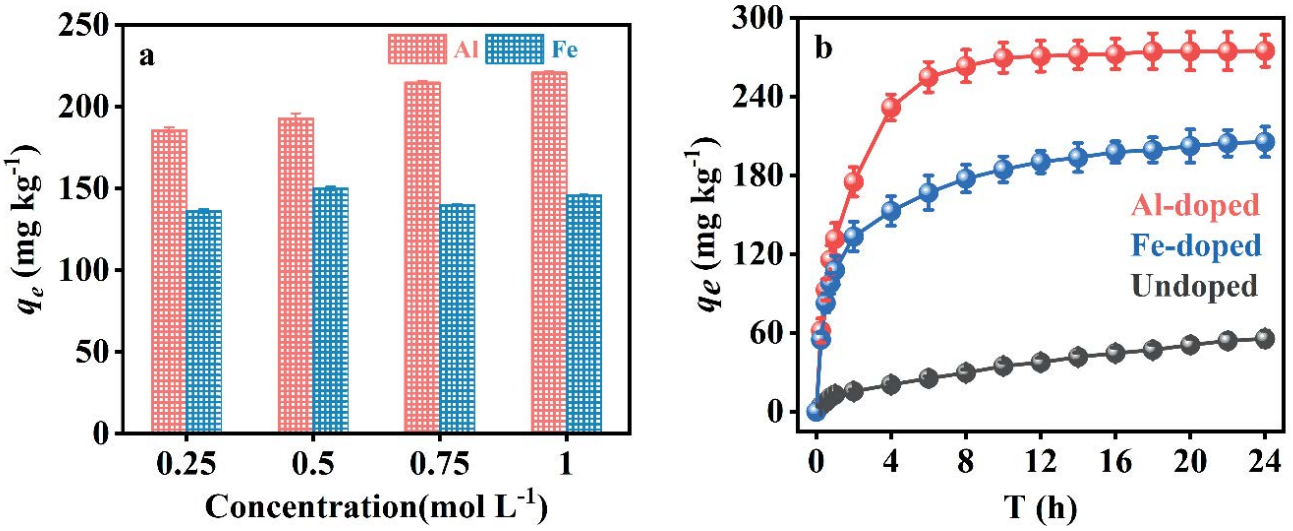

Fig. 3. Influence of concentration of doped metal solution on adsorption effect (a) and adsorption equilibrium capacity of phosphorus at different reaction times (b).

ions can directly affect the iron-phosphorus cycle [6,20]. Therefore, Al-doped ceramsite had the best phosphorus removal effect.

Coal cinder was an inorganic waste produced by coal combustion [21]. The adsorption capacity of phosphorus is shown in Table 2. The results reflected that the adsorption capacity of Al and Fe-doped ceramsite in this study was higher than that of coal cinder. Thus, Al and Fe salt doping waste-based ceramsite can effectively remove phosphorus from industrial wastewater.

Many untreated solid wastes such as fly ash (FA) [8,22], sewage sludge (SS) [23,24], etc. have been investigated for phosphorus removal. In this study, the mixture of FA, SS, and concrete was used to prepare ceramsite to adsorb phosphorus from industrial wastewater. Table 3 shows that the phosphorus removal capacity of the composite material is higher than that of FA and SS (its phosphorus removal capacity is as high as 99%). The adsorption capacity of the composite prepared in this study was lower than that of single materials (e.g., FA and SS). This phenomenon may be because that FA and SS are in powder form, while the concrete incorporated in this study is in block form, which has fewer adsorption sites and a smaller specific surface area. However, the use of FA, SS, and concrete to prepare ceramic adsorbent achieves the purpose of waste to waste.

Table 2
Similar results about P adsorption of porous materials

Adsorbent	P adsorption q_{max} (mg kg^{-1})	Reference
Coal cinder	398	Yang et al. [21]
Fe-doped ceramsite	458.26	This study
Al-doped ceramsite	669.1	This study

3.3. Characterization of Al and Fe-doped ceramsite

3.3.1. SEM and EDS

The surface morphology of undoped, Al and Fe-doped ceramsite was observed by SEM, as shown in Fig. 4. The surface of three kinds of ceramsite presented a massive crystalline molten state, with rough surfaces and many internal pores (Fig. 4a–c). This might be because there was a higher carbon content in fly ash and more organic matter in the sludge. And these organics reacted with gases under high-temperature conditions. Among them, the carbon in the sludge mainly existed in the form of volatile compounds, which provided sufficient material for the expansion of ceramsite. These gas-forming substances made ceramsite generate enough gas during the sintering process to escape the surface of ceramsite. As a result, the pores inside the ceramsite were not uniform and the specific surface area was larger, which provided more active sites for attaching metal ions during the doping process. Thereby improving the adsorption performance of ceramsite to harmful substances in industrial wastewater [25,26].

Combined with the EDS, the main elements of ceramsite were C, O, Al, Si, Fe, Mg, and Ca. That is, the main components were SiO_2 and Al_2O_3. What's more, it can be found that the elemental composition of undoped ceramsite was C (7.87%), O (44.33%), Al (7.92%), Si (17.69%), Fe (1.45%), Mg (4.48%), Ca (14%) (Fig. 4d). Fe-doped ceramsite had its elemental composition C (7.94%), O (44.44%), Al (11.61%), Si (19.08%), Fe (9.1%), Mg (1.62%), Ca (3.02%) (Fig. 4e). Besides, the element composition of Al-doped ceramsite was C (8.66%), O (46.11%), Al (15.82%), Si (18.38%), Fe (1.81%), Mg (2.48%), Ca (3.79%) (Fig. 4f). By comparing before and after doping, it was obvious that Al element increased from 7.92% to 15.82%, Fe element raised from 1.45% to 9.1%. The content of Al in Al-doped ceramsite was higher than that in undoped ceramsite, and the Fe in Fe-doped ceramsite was also higher than that in undoped ceramsite, indicating that the doping method in this experiment was valid.

Table 3
Summary of phosphorus removal performance of various industrial wastes

Material	Dosage (g L^{-1})	pH	Initial P (mg P L^{-1})	P removal (%)	P adsorption capacity (mg P kg^{-1})	Reference
Alum SS	1		14.7	42	174	Razali et al. [23]
FA	20	–	100	82	4,100	Lu et al. [22]
SS	10	7	5	29	145	Mohammed and Rashid [24]
FA	8	–	100	50	6,280	Wang et al. [8]
FA, SS, concrete	40	7	10	99	280	This study

3.3.2. X-ray diffraction

The chemical composition of ceramsite was determined by XRD-6100 X-ray Fluorescence Analyzer (XRD) and a semi-quantitative analysis method was chosen. The XRD diffraction patterns of undoped, Al and Fe-doped ceramsite are shown in Fig. 4g. The components of undoped, Al and Fe-doped ceramsite all contained quartz crystals (SiO_2). However, compared with the results of EDS elemental analysis, XRD did not detect the actual presence of CaO, Al_2O_3, Fe_2O_3, and other components in the doped ceramsite. This phenomenon may be due to certain crystal defects in the crystal structure formed by Al and Fe salts doping in the ceramsite. Furthermore, Al^{3+}, Fe^{3+}, and Ca^{2+} can provide active sites when doped ceramsite adsorbs and react with PO_4^{3-} for ion exchange and surface precipitation [27,28].

3.3.3. FTIR spectra

The FTIR is a kind of spectrum that shows molecular vibration, which purpose is to identify or distinguish the properties of organic materials, such as polymers, lubricants, adhesives, and cleaning agents.

As shown in Fig. 4h, the absorption peaks at 3,430 and 918 cm^{-1} in the undoped, Al and Fe-doped ceramsite were associated with stretching vibration of the surface hydroxyl (–OH). Meanwhile, the stretching vibration of the aromatic C=C group caused the absorption peak at 1,630 cm^{-1}. There was a strong and broad peak between 1,000 and 1,200 cm^{-1}, with a main maximum adsorption peak at 1,070 cm^{-1}. This phenomenon might be due to the O–Si–O bond's stretching vibration and the Si–O–Si bond's asymmetric stretching vibration [23]. The characteristic infrared peak of Al–O at 764 cm^{-1} and the distinct peak at 565 cm^{-1} was attributed to the stretching vibration band of Fe–O [29]. Therefore, three kinds of ceramsite contained Al_2O_3, Fe_2O_3, and other metal oxides, which can perform ion exchange with phosphate and surface precipitation.

3.4. Adsorption kinetics and adsorption isotherm

3.4.1. Adsorption kinetics

To further grasp the change rule of the adsorption capacity with time, adsorption kinetics was studied. The first-order and second-order kinetic models were fitted to the relationship of three kinds of ceramsite adsorption capacity with time. The kinetic fitting line is shown in Fig. 5, and the appropriate kinetic parameters are shown in Table 4.

Fig. 5a and b show the first-order and the second-order kinetic model of three kinds of ceramsite adsorption processes, respectively. Two kinetic models could fit the process of adsorbing phosphorus by Al and Fe-doped ceramsite. It is worth noting that the second-order kinetic model showed a better result (r^2>0.98) for high concentration phosphorus (10 mg L^{-1}) compared to the first-order kinetic model, and the predicted q_e based on the secondary kinetic model was relatively close to the experimentally measured $q_{e,\exp}$. This might be the fact that the second-order kinetic model was based on the bilayer adsorption theory, which included multiple adsorption processes such as external liquid film diffusion and surface adsorption, and chemical reactions played an important role in the adsorption process [30]. Hence the rate controlling step for phosphorus adsorption was a chemical interaction [31].

3.4.2. Adsorption isotherm

The adsorption equilibrium isotherm was used to describe the distribution of adsorbate molecules between the liquid and solid phases in the equilibrium state [32]. Isothermal simulation of phosphorus adsorption by three kinds of ceramsite in solution is shown in Fig. 5c–e, the predicted isotherm parameters shown in Table 5. The Langmuir adsorption isotherm model better explained the adsorption of phosphorus by Al and Fe-doped ceramsite with the highest correlation coefficient compared to the Freundlich simulation. The Langmuir model shows monolayer phosphorus adsorption in solution on the surface of uniform Al and Fe-doped ceramsite [33]. The Al-doped ceramsite showed the highest adsorption capacity of 669.1 mg kg^{-1}, followed by Fe-doped ceramsite with 458.26 mg kg^{-1}. In general, Al and Fe-doped ceramsite could effectively remove phosphorus from industrial wastewater, with Al-doped ceramsite showing the best adsorption effect. The experimental result was consistent with Angaru et al. [33–35], which indicated that the Langmuir model had a slightly better fitting performance than the Freundlich models, which indicated that the Langmuir model had a slightly better fitting performance than the Freundlich models.

3.5. XPS and FTIR of doped ceramsite before and after adsorption

Fig. 6a–c show the X-ray photoelectron spectroscopy (XPS) patterns of undoped, Al and Fe-doped ceramsite before and after P adsorption. Only a $2p_{3/2}$ peak was detected in undoped ceramsite, and the binding energy

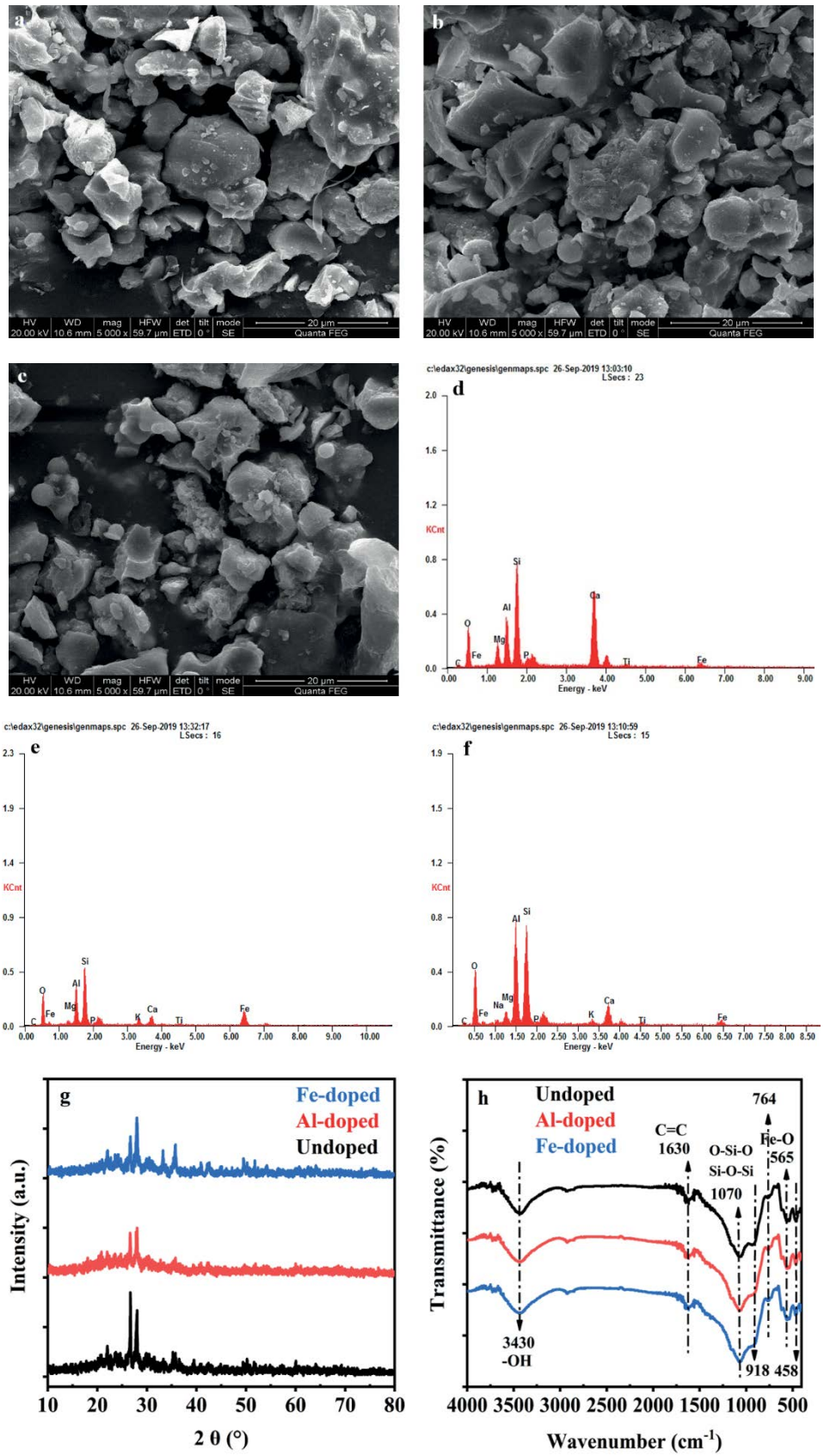

Fig. 4. SEM images (a–c) and EDS (d–f) of three kinds of ceramsite. XRD patterns (g) and FTIR spectra (h) of three kinds of ceramsite (a and d) undoped ceramsite, (b and e) Fe-doped ceramsite and (c and f) Al-doped ceramsite.

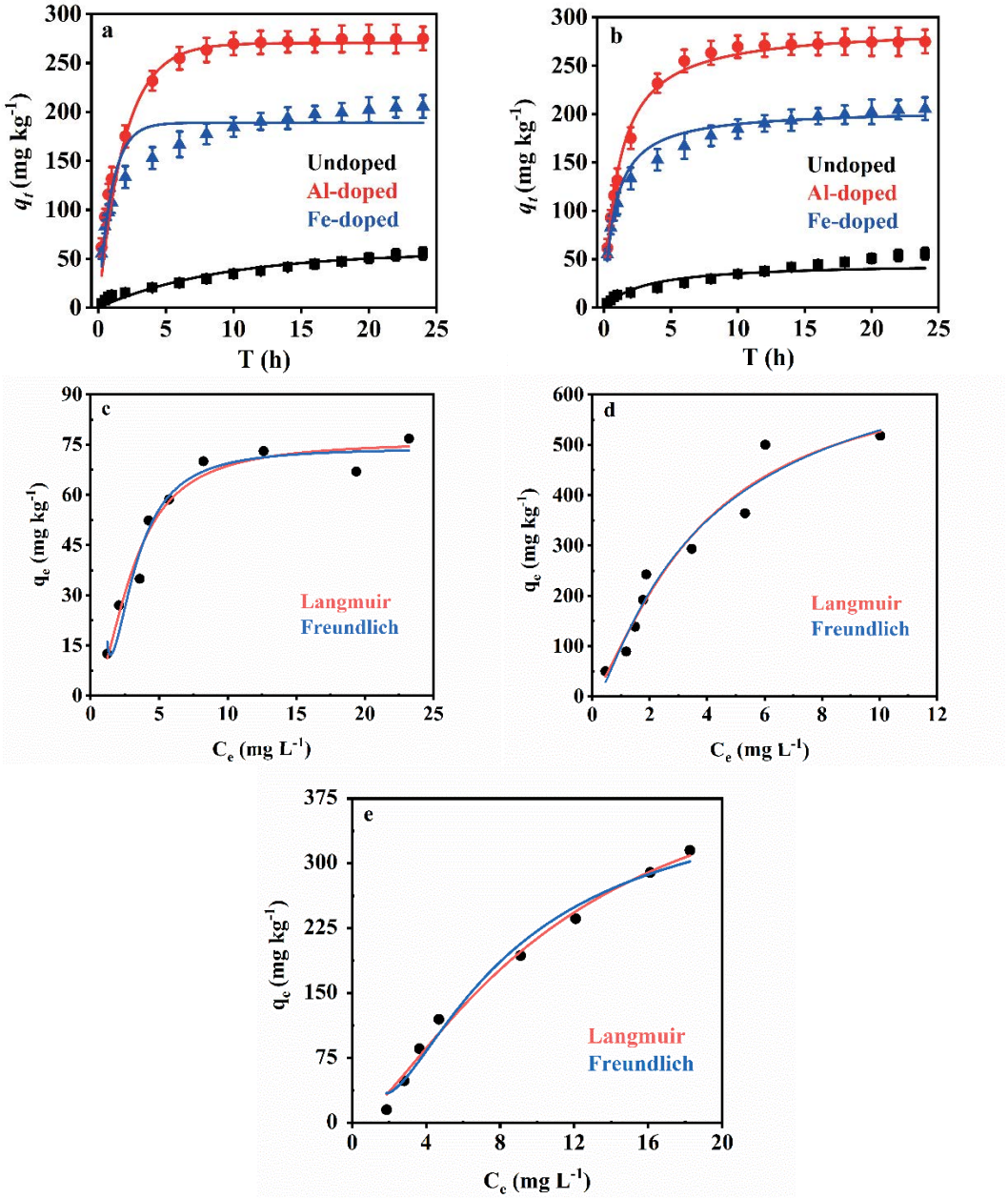

Fig. 5. Kinetic model (a) first-order kinetic model and (b) second-order kinetic model of phosphorus adsorption by three kinds of ceramsite. Isothermal simulation of phosphorus adsorption by three kinds of ceramsite in solution (c) undoped ceramsite, (d) Al-doped ceramsite and (e) Fe-doped ceramsite. (Experimental conditions: the initial phosphate concentration: 10 mg L^{-1}, the dosage of undoped ceramsite: 100 g L^{-1}, the dosage of Al and Fe-doped ceramsite: 40 g L^{-1}, the temperature: 25°C).

Table 4
Relative parameters of adsorption kinetics equation for phosphorus removal (mg kg^{-1})

Doping methods	$q_{e,exp}$ (mg kg^{-1})	First-order kinetic models			Second-order kinetic models		
		q_e (mg kg^{-1})	k_1 (h^{-1})	r^2	q_e (mg kg^{-1})	k_2 (h^{-1})	r^2
Undoped	55.62	56.467	0.097	0.800	45.982	0.007	0.924
Al	274.87	267.08	0.515	0.956	280.536	0.003	0.995
Fe	205.55	188.911	0.845	0.939	205.000	0.006	0.986

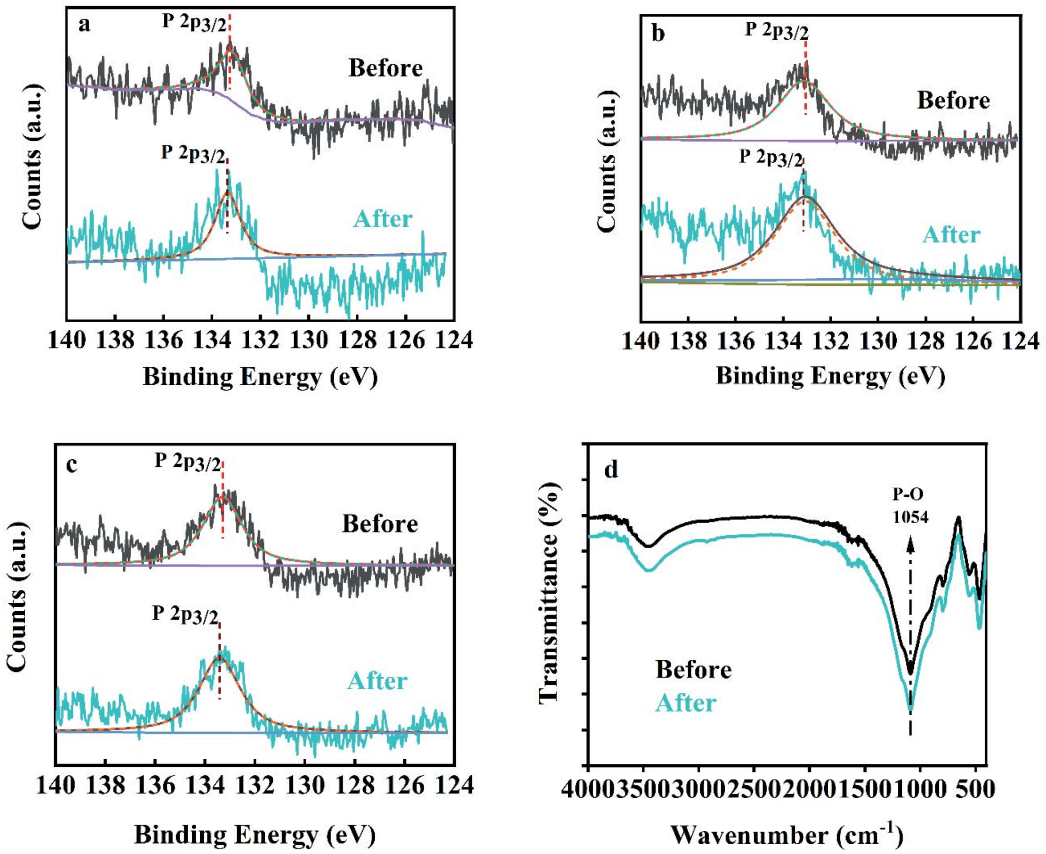

Fig. 6. Before and after phosphorus adsorption by undoped ceramsite (a), Al-doped ceramsite (b) and Fe-doped ceramsite (c), FTIR spectra before and after phosphorus adsorption by Al-doped ceramsite (d).

of this peak before and after adsorption was centered at 133.25 and 133.40 eV, respectively. For Al-doped ceramsite, the binding energy of the P-element before adsorption was centered at 133.05 eV, and after adsorption, it is centered at 133.15 eV. The binding energy of p-element before and after adsorption of Fe-doped ceramsite was centered at 133.25 and 133.45 eV, respectively. Comparing the undoped, Al and Fe-doped ceramsite after adsorption, it can be found that the peak area of the P element increased to some extent, which indicates that the Al and Fe-doped ceramsite improve the adsorption capacity of P. Fig. 6d shows the FTIR spectra of Al-doped ceramsite before and after adsorption, and it was observed that the Al-doped ceramsite showed P–O groups at a wavelength of 1,054 cm^{-1}. In addition, the increase of P–O groups at this wavelength after the adsorption of P by Al-doped ceramsite can further prove that Al-doped ceramsite improves their adsorption of P in solution.

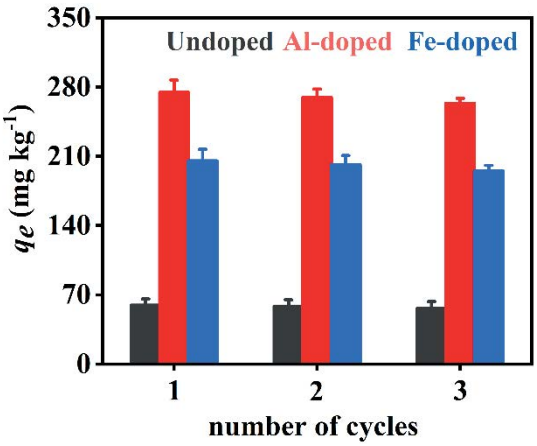

Fig. 7. Reusability performance of Al and Fe-doped ceramsite at three cycles.

3.6. Recyclability

After phosphorus adsorption, the recyclability of Al and Fe-doped ceramsite was facilitated by treatment with NaOH solution. This was because the stable solid phases of aluminum and iron phosphate present on the surface of the ceramsite combine with OH^- ions in the solution to produce complexes or precipitates of aluminum hydroxide and iron hydroxide while releasing PO_4^{3-}, HPO_4^{2-}, and $H_2PO_4^-$ into the solution during the reaction [36]. Fig. 7 examines the adsorption effect of Al and Fe-doped ceramsite at three cycles. The phosphorus removal capacity of the adsorbent decreases slightly with the number of repeated uses, and its

Table 5
Langmuir and Freundlich adsorption isotherm of three kinds of ceramsite

Doping methods	Freundlich			Langmuir		
	k_F	n	r^2	q_{max}	k_L	r^2
Undoped	73.928	2.679	0.95	76.085	0.119	0.96
Al	97.587	0.176	0.952	669.1	0.177	0.953
Fe	398.38	1.631	0.984	458.26	0.031	0.991

adsorption efficiency is below 95% after a maximum of three repeated uses. A small amount of P concentration remained on the surface or in the internal pores of the Al and Fe-doped ceramsite during each reuse cycle and occupied the active site, resulting in a slight decrease in removal capacity.

4. Conclusions

This study demonstrated that Al and Fe-doped ceramsite could effectively remove phosphorus in wastewater. The best ceramsite ratio with fly ash, sewage sludge, and concrete as raw materials were 6:3:2. When the concentration of Al and Fe salt were 0.75 mol L^{-1} respectively, Al and Fe-doped ceramsite had a better phosphorus adsorption effect. The optimal reaction time of Al and Fe-doped ceramsite was 20 h, and the phosphorus removal effect of Al-doped ceramsite was better than that of Fe-doped ceramsite. In addition, the second-order kinetic model was more suitable for describing the adsorption of Al and Fe-doped ceramsite to phosphorus. The adsorption of Al and Fe-doped ceramsite to phosphorus could be well fitted by the Langmuir model. This study developed Al and Fe-doped ceramsite that adsorb phosphorus in wastewater, which provided a strategy for the practical application of waste such as fly ash/sewage sludge/concrete.

Acknowledgements

The authors would like to acknowledge and appreciate the Natural Science Fund Project of Colleges in Jiangsu Province (20KJB610010), the start-up foundation for introducing talent of NUIST and National key R&D program of China (2018YFD0900805).

Conflict of interest

The authors declare no conflict of interest.

References

[1] M. Ilyas, W. Ahmad, H. Khan, S. Yousaf, M. Yasir, A. Khan, Environmental and health impacts of industrial wastewater effluents in Pakistan: a review, Rev. Environ. Health, 34 (2019) 171–186.
[2] C.J. Liu, Y.Z. Li, Z.K. Luan, Z.Y. Chen, Z.G. Zhang, Z.P. Jia, Adsorption removal of phosphate from aqueous solution by active red mud, J. Environ. Sci., 19 (2007) 1166–1170.
[3] C. Wang, W. Guo, B. Tian, Y. Pei, K. Zhang, Characteristics and kinetics of phosphate adsorption on dewatered ferric-alum residuals, J. Environ. Sci. Health. Part A Toxic/Hazard. Subst. Environ. Eng., 46 (2011) 1632–1639.
[4] W. Xiong, J. Tong, Z. Yang, G. Zeng, Y. Zhou, D. Wang, M. Cheng, Adsorption of phosphate from aqueous solution using iron-zirconium modified activated carbon nanofiber: performance and mechanism, J. Colloid Interface Sci., 493 (2017) 17–23.
[5] M. El Bouraie, A.A. Masoud, Adsorption of phosphate ions from aqueous solution by modified bentonite with magnesium hydroxide $Mg(OH)_2$, Appl. Clay Sci., 140 (2017) 157–164.
[6] X. Wang, B.L. Phillips, J.F. Boily, Y. Hu, Z. Hu, P. Yang, M. Zhu, Phosphate sorption speciation and precipitation mechanisms on amorphous aluminum hydroxide, Soil Syst., 3 (2019) 20, doi: 10.3390/soilsystems3010020.
[7] S. Moharami, M. Jalali, Removal of phosphorus from aqueous solution by Iranian natural adsorbents, Chem. Eng. J., 223 (2013) 328–339.
[8] Y. Wang, Y. Yu, H. Li, C. Shen, Comparison study of phosphorus adsorption on different waste solids: fly ash, red mud and ferric-alum water treatment residues, J. Environ. Sci., 50 (2016) 79–86.
[9] Q. Hou, P. Meng, H. Pei, W. Hu, Y. Chen, Phosphorus adsorption characteristics of alum sludge: adsorption capacity and the forms of phosphorus retained in alum sludge, Mater. Lett., 229 (2018) 31–35.
[10] G. Cheng, Q. Li, Z. Su, S. Sheng, J. Fu, Preparation, optimization, and application of sustainable ceramsite substrate from coal fly ash/waterworks sludge/oyster shell for phosphorus immobilization in constructed wetlands, J. Cleaner Prod., 175 (2018) 572–581.
[11] F.O. Ochedi, Y. Liu, A. Hussain, A review on coal fly ash-based adsorbents for mercury and arsenic removal, J. Cleaner Prod., 267 (2020) 122143, doi: 10.1016/j.jclepro.2020.122143.
[12] S. Li, R.A. Cooke, L. Wang, F. Ma, R. Bhattarai, Characterization of fly ash ceramic pellet for phosphorus removal, J. Environ. Manage., 189 (2017) 67–74.
[13] Y. Chen, J. Shi, H. Rong, X. Zhou, F. Chen, X. Li, T. Wang, H. Hou, Adsorption mechanism of lead ions on porous ceramsite prepared by co-combustion ash of sewage sludge and biomass, Sci. Total Environ., 702 (2020) 135017, doi: 10.1016/j.scitotenv.2019.135017.
[14] J.Z. Liu, R. Liu, Z.M. He, M.F. Ba, Y.S. Li, Preparation and microstructure of green ceramsite made from sewage sludge, J. Wuhan Univ. Technol.-Mater. Sci. Ed., 27 (2012) 149–153.
[15] C. Martínez-García, D. Eliche-Quesada, L. Pérez-Villarejo, F.J. Iglesias-Godino, F.A. Corpas-Iglesias, Sludge valorization from wastewater treatment plant to its application on the ceramic industry, J. Environ. Manage., 95 (2012) S343–S348.
[16] Z. Li, X. Liu, Y. Wang, Modification of sludge-based biochar and its application to phosphorus adsorption from aqueous solution, J. Mater. Cycles Waste Manage., 22 (2020) 123–132.
[17] B. Zhang, X. Wang, S. Li, Y. Liu, Y. An, X. Zheng, Preferable adsorption of nitrogen and phosphorus from agricultural wastewater using thermally modified zeolite–diatomite composite adsorbent, Water, 11 (2019) 2053, doi: 10.3390/w11102053.
[18] J.Q. Gao, J. Zhao, J.S. Zhang, Q. Li, J.L. Gao, M. Cai, J.L. Zhang, Preparation of a new low-cost substrate prepared from drinking water treatment sludge (DWTS)/bentonite/zeolite/fly ash for rapid phosphorus removal in constructed wetlands, J. Cleaner Prod., 261 (2020) 121110, doi: 10.1016/j.jclepro.2020.121110.
[19] H. Huo, H. Lin, Y. Dong, H. Cheng, H. Wang, L. Cao, Ammonia-nitrogen and phosphates sorption from simulated reclaimed waters by modified clinoptilolite, J. Hazard. Mater., 229 (2012) 292–297.
[20] F. Gérard, Clay minerals, iron/aluminum oxides, and their contribution to phosphate sorption in soils — a myth revisited, Geoderma, 262 (2016) 213–226.
[21] J. Yang, S. Wang, Z. Lu, J. Yang, S. Lou, Converter slag-coal cinder columns for the removal of phosphorous and other pollutants, J. Hazard. Mater., 168 (2009) 331–337.
[22] S.G. Lu, S.Q. Bai, L. Zhu, H.D. Shan, Removal mechanism of phosphate from aqueous solution by fly ash, J. Hazard. Mater., 161 (2009) 95–101.

[23] M. Razali, Y.Q. Zhao, M. Bruen, Effectiveness of a drinking-water treatment sludge in removing different phosphorus species from aqueous solution, Sep. Purif. Technol., 55 (2007) 300–306.
[24] W.T. Mohammed, S.A. Rashid, Phosphorus removal from wastewater using oven-dried alum sludge, Int. J. Chem. Eng., 2012 (2012) 125296, doi: 10.1155/2012/125296.
[25] J. Qin, C. Cui, X. Cui, A. Hussain, C. Yang, Preparation and characterization of ceramsite from lime mud and coal fly ash, Constr. Build. Mater., 95 (2015) 10–17.
[26] T. Li, T. Sun, D. Li, Preparation, sintering behavior, and expansion performance of ceramsite filter media from dewatered sewage sludge, coal fly ash, and river sediment, J. Mater. Cycles Waste Manage., 20 (2018) 71–79.
[27] W. Huang, Y. Zhang, D. Li, Adsorptive removal of phosphate from water using mesoporous materials: a review, J. Environ. Manage., 193 (2017) 470–482.
[28] L. Dai, F. Tan, H. Li, N. Zhu, M. He, Q. Zhu, G. Hu, L. Wang, J. Zhao, Calcium-rich biochar from the pyrolysis of crab shell for phosphorus removal, J. Environ. Manage., 198 (2017) 70–74.
[29] H. Zhou, Z. Jiang, S. Wei, A novel absorbent of nano-Fe loaded biomass char and its enhanced adsorption capacity for phosphate in water, J. Chem., 2013 (2013) 649868, doi: 10.1155/2013/649868.
[30] J. Zhao, Y. Niu, B. Ren, H. Chen, S. Zhang, J. Jin, Y. Zhang, Synthesis of Schiff base functionalized superparamagnetic Fe_3O_4 composites for effective removal of Pb(II) and Cd(II) from aqueous solution, Chem. Eng. J., 347 (2018) 574–584.
[31] L.P. Lingamdinne, R.R. Karri, M.R. Khan, Y.Y. Chang, J.R. Koduru, Evaluation of surface phenomena of magnetic biomass for dye removal via surface modeling, J. Environ. Chem. Eng., 9 (2021) 105953, doi: 10.1016/j.jece.2021.105953.
[32] C.A.P. Almeida, N.A. Debacher, A.J. Downs, L. Cottet, C.A.D. Mello, Removal of methylene blue from colored effluents by adsorption on montmorillonite clay, J. Colloid Interface Sci., 332 (2009) 46–53.
[33] G.K.R. Angaru, L.P. Lingamdinne, Y.L. Choi, J.R. Koduru, J.K. Yang, Y.Y. Chang, Encapsulated zerovalent iron/nickel-fly ash zeolite foam for treating industrial wastewater contaminated by heavy metals, Mater. Today Chem., 22 (2021) 100577, doi: 10.1016/j.mtchem.2021.100577.
[34] K. Narasimharao, L.P. Lingamdinne, S. Al-Thabaiti, M. Mokhtar, A. Alsheshri, S.Y. Alfaifi, Y.-Y. Chang, J.R. Koduru, Synthesis and characterization of hexagonal Mg–Fe layered double hydroxide/grapheme oxide nanocomposite for efficient adsorptive removal of cadmium ion from aqueous solutions: isotherm, kinetic, thermodynamic and mechanism, J. Water Process Eng., 47 (2022) 102746, doi: 10.1016/j.jwpe.2022.102746.
[35] G.K.R. Angaru, Y.L. Choi, L.P. Lingamdinne, J.R. Koduru, J.K. Yang, Y.Y. Chang, R.R. Karri, Portable SA/CMC entrapped bimetallic magnetic fly ash zeolite spheres for heavy metals contaminated industrial effluents treatment via batch and column studies, Sci. Rep., 12 (2022) 1–17.
[36] X. Liu, Y. Wang, R.L. Smith, J. Fu, X. Qi, High-capacity structured MgO-Co adsorbent for removal of phosphorus from aqueous solutions, Chem. Eng. J., 426 (2021) 131381, doi: 10.1016/j.cej.2021.131381.